

**Numerical Approaches to High Energy Electroweak  
Baryon Number Violation  
Above and Below the Sphaleron Barrier** \*

Claudio Rebbi <sup>†</sup>

*Physics Department  
Boston University  
590 Commonwealth Avenue  
Boston, MA 02215, USA*

Robert Singleton, Jr. <sup>‡</sup>

*Physics Department  
The University of Washington  
Box 351560  
Seattle, WA 98195, USA*

**Abstract**

We review some promising numerical techniques for calculating high energy baryon number violating cross sections in the standard model. As these lectures are designed to be self-contained, we present in some detail the formalism of Rubakov, Son, and Tinyakov, which provides a means of bounding the two-particle cross sections in a semi-classical manner. The saddle-point solutions required by this method must be found computationally and are of two basic types, corresponding to tunneling events between adjacent topological sectors on the one hand, and classically allowed evolution over the sphaleron barrier on the other. In both cases one looks for topology changing solutions of small incident particle number. In the classically allowed regime we have developed a Monte Carlo technique that systematically lowers the particle number while still ensuring that a change in topology takes place. We also make progress towards a numerical method amenable for the more computationally challenging problem of finding the complexified tunneling solutions, and we present some of our numerical findings, both above and below the sphaleron barrier.

BUHEP-96-36    UW/PT 96-21  
hep-ph/9706424

Typeset in LaTeX

---

\*This paper is based on talks given by C. Rebbi and R. Singleton at the 1996 Summer School on Cosmology and High Energy Physics, held at ICTP in Trieste, Italy.

<sup>†</sup>rebbi@pthind.bu.edu

<sup>‡</sup>bobs@terrapin.phys.washington.edu

## I. INTRODUCTION

The prospect [1,2] of observable baryon number violation in high energy electroweak collisions has provoked much excitement, but despite considerable effort, it has not been possible to obtain conclusive evidence that unsuppressed baryon number violation can indeed occur at energies in the multi-TeV range. The purpose of this paper is to summarize some recent developments which offer hope for a reliable calculation of the magnitude of baryon number violating cross sections.

Limitations of space do not permit a comprehensive treatment of this vast subject. These lectures will focus on the semiclassical methods introduced in Refs. [3] and [4] and further work by the present authors. The main idea in Refs. [3] and [4] consists in studying processes with energy and initial particle number of the form  $E = \epsilon/g^2$  and  $N_i = \nu/g^2$ , with  $g$  being the electroweak coupling constant, in the limit where  $g \rightarrow 0$  while  $\epsilon$  and  $\nu$  are held fixed. Under such conditions one can justify the use of semiclassical methods to extract the exponential behavior of the semi-exclusive cross section, which can be done by calculating hybrid Euclidean-Minkowski solutions which violate baryon number via tunneling from one (non-vacuum) real-time configuration to another. Finding such semiclassical solutions is however highly non-trivial and can only be done by computational methods. In Ref. [3] we have applied numerical techniques to the study of processes in which the gauge and Higgs fields change their topology through purely classical evolution, thus inducing a violation of baryon number. The investigation of the semiclassical solutions that account for tunneling under the barrier is in progress.

These two approaches, one involving classically forbidden tunneling-like processes and the other classically allowed topological transitions, probe complementary aspects of the problem and should produce compatible results (thereby providing consistency

checks). Both approaches require solutions to certain nonlinear partial differential equations for which no (nontrivial) exact solutions are known; however, these equations are well suited to computational study and one can still make considerable progress. Along with P. Tinyakov, we have recently launched a numerical investigation of the standard model baryon number violating rates based on Ref. [4], and in the next section we shall review the relevant formalism and present some of our initial results. The rest of this paper is devoted to the numerical work of Ref. [3]. We presently have much more to say about this approach because its corresponding computational study is at a mature stage of development. Finally, in an effort to write a self contained work, the remainder of this introduction is devoted to a brief exposition of nonperturbative baryon number violation in the standard model of electroweak interactions.

For our purposes, when we talk of the “standard model” we mean the standard model in which the Weinberg angle has been set to zero, i.e. we shall be considering  $SU(2)$  gauge theory spontaneously broken via a single Higgs doublet. This simplified model has all the relevant physics. Most important, the gauge structure dictates nontrivial topology for the bosonic vacuum sector. Working in the temporal gauge with periodic boundary conditions at spatial infinity, each vacuum may be characterized by an integer called the winding number which measures the number of times the gauge manifold is wound around 3-space [5]. As this number is a topological invariant, vacua of different winding numbers cannot be continuously deformed into one another.

Because of the axial vector anomaly, baryon number violation occurs when the gauge and Higgs fields change their topology [6]. Adjacent topological sectors are separated by an extremely high barrier, the top of which is a static saddle-point solution to the equations of motion. This configuration is called the sphaleron [7],

and it has an energy of about 10 TeV and possesses a single unstable direction in field space. At low energy the baryon number violating rates are exceedingly small, as the gauge and Higgs fields must first tunnel through the sphaleron, which is indeed extremely unlikely.

Recently, the prospect of rapid baryon number violation at high temperatures and high energies has emerged. The basic idea is that if the gauge and Higgs fields have enough energy, they can change their topology by sailing over the sphaleron barrier rather than being forced to tunnel through it. At high temperatures this is precisely what happens, and it is generally agreed that baryon number violation becomes unsuppressed in the early universe [8].

The situation in high energy collisions is far less clear. The limiting process in baryon number violation is the production of a sphaleron-like configuration from an incident beam of high energy particles. But since the sphaleron is a large extended object, there is a scale mismatch with the initial high energy two-particle state, and hence one naively expects the baryon number violating rate to be small. However, Ringwald [1] and Espinosa [2] have suggested that the sum over many-particle final states gives rise to factors that grow with energy sufficiently rapidly to offset any exponential suppression. If true, this offers the exciting prospect of one day observing baryon number violation in high energy collisions.

## II. THE CLASSICALLY FORBIDDEN DOMAIN

The approach of Ringwald and Espinosa [1,2], however, neglects some important corrections which still elude calculation despite considerable effort. Apart from lattice simulations, semi-classical techniques are our only handle on nonperturbative effects. The basic problem with calculating the anomalous baryon number violating cross

sections is that exclusive two-particle initial states are not very amenable to these methods, and there are potentially large initial state corrections whose effects remain undetermined.

Rather than calculating the two-particle cross section directly, Rubakov, Son and Tinyakov [4] investigate a related quantity for which semiclassical methods are still applicable. Their method involves saturating the path integral representation of this quantity with a complexified Euclidean-Minkowski saddle-point. This solution includes the effects of tunneling under the sphaleron barrier, and is a generalization of the periodic instanton of Ref. [9]. We now review in more detail the work of Ref. [4], along with selected portions of Refs. [9] – [12] upon which this work is based.

### A. The Inclusive Cross Section

As previously mentioned, the calculations of Refs. [1] and [2] for the two-particle baryon number violating cross section,  $\sigma_2(E)$ , become unreliable at high energy. This is because of a failure of semiclassical methods in calculating exclusive quantities like two-particle scattering amplitudes. So rather than calculating  $\sigma_2(E)$  directly, Ref. [4] examines a related *inclusive* quantity:

$$\sigma(E, N) = \sum_{f,i} |\langle f | \hat{S} \hat{P}_E \hat{P}_N | i \rangle|^2, \quad (2.1)$$

where the sum is over all initial and final states,  $\hat{S}$  is the  $S$ -matrix, and  $\hat{P}_E$  and  $\hat{P}_N$  are projection operators onto subspaces of energy  $E$  and particle number  $N$  respectively.

Unlike the exclusive two-particle cross section,  $\sigma(E, N)$  is directly calculable by semiclassical methods as long as the incident particle number  $N$  remains large. If the energy and particle number are parameterized by

$$E = \frac{\epsilon}{g^2} \quad (2.2a)$$

$$N = \frac{\nu}{g^2}, \quad (2.2b)$$

and the fields are rescaled by appropriate powers of  $g^2$ , then in the limit  $g \rightarrow 0$  with  $\epsilon$  and  $\nu$  held fixed, the path integral for  $\sigma(E, N)$  can be saturated by a  $g$ -independent classical saddle-point solution to the equations of motion. As shown in the next section, the cross section takes the form

$$\sigma(E, N) = \exp \left[ \frac{1}{g^2} F(\epsilon, \nu) + \mathcal{O}(g^0) \right] , \quad (2.3)$$

where the function  $F(\epsilon, \nu)$  is determined by the classical solution.

The utility of  $\sigma(E, N)$  is that it may be used to bound the two-particle cross section and allow one to extract the exponential behavior of  $\sigma_2(E)$ . By construction,  $\sigma(E, N)$  provides an upper bound to  $\sigma_2(E)$ . This is because one of the initial  $N$ -particle states of (2.1) possesses  $N - 2$  free propagating particles and two colliding particles [11]. A lower bound may be obtained under some reasonable physical assumptions [13]. Let  $|\psi_N \rangle$  be the initial state that saturates the sum in (2.1). If the process  $2 \rightarrow \text{any}$  proceeds through some preferred intermediate state, such as a sphaleron-like configuration in the case of baryon number violation, then the substitution of this state by  $|\psi_N \rangle$  will underestimate the result, giving the inequality  $|\langle \psi_N | 2 \rangle|^2 \sigma(E, N) < \sigma_2(E)$ . Estimating  $|\langle \psi_N | 2 \rangle|^2 \sim \exp(-\text{const } N)$ , together with the previous upper bound, gives the inequalities

$$\exp(-\text{const } N) \sigma(E, N) < \sigma_2(E) < \sigma(E, N) , \quad (2.4)$$

from which it follows that

$$\lim_{g \rightarrow 0} g^2 \ln \sigma_2(E) = F(\epsilon, \nu) + \mathcal{O}(\nu) . \quad (2.5)$$

The consistency of the first inequality requires that  $F(\epsilon, \nu)$  has a smooth  $\nu \rightarrow 0$  limit, in which case  $F(\epsilon, 0)$  determines the exponential behavior of  $\sigma_2(E)$ . However, the second inequality of (2.4) holds regardless of continuity, and hence if  $\sigma(E, N)$  is exponentially suppressed (for any value of  $N$ ), then so is  $\sigma_2(E)$ .

## B. Development of the Formalism

We now review the formalism developed in Ref. [4] used to calculate the inclusive-state cross section  $\sigma(E, N)$ . For purposes of illustration, we consider a system with a single real scalar field, whose field operator  $\hat{\phi}(\mathbf{x})$  has eigenstates defined by  $\hat{\phi}(\mathbf{x})|\phi\rangle = \phi(\mathbf{x})|\phi\rangle$ . The approach that follows is based on a coherent state formalism, where coherent states  $|a\rangle$  are defined by  $\hat{a}_{\mathbf{k}}|a\rangle = a_{\mathbf{k}}|a\rangle$ , with  $\hat{a}_{\mathbf{k}}$  being the annihilation operator of the  $\mathbf{k}$ -th mode. In field space the coherent states take the form

$$\langle\phi|a\rangle = \text{const} \cdot \exp\left[\int d^3k \left\{-\frac{1}{2}a_{\mathbf{k}}a_{-\mathbf{k}} - \frac{1}{2}\omega_{\mathbf{k}}\phi(\mathbf{k})\phi(-\mathbf{k}) + \sqrt{2\omega_{\mathbf{k}}}a_{\mathbf{k}}\phi(\mathbf{k})\right\}\right], \quad (2.6)$$

where  $\phi(\mathbf{k})$  is the spatial Fourier transform of  $\phi(\mathbf{x})$ , given by

$$\phi(\mathbf{x}) = \int \frac{d^3k}{(2\pi)^{3/2}} e^{i\mathbf{k}\cdot\mathbf{x}} \phi(\mathbf{k}). \quad (2.7)$$

In the coherent state formalism, the  $S$ -matrix is represented by its kernel  $S(b^*, a) \equiv \langle b|\hat{S}|a\rangle$ , and inserting a complete set of field-states we can write

$$S(b^*, a) = \int \mathcal{D}\phi_i(\mathbf{x})\mathcal{D}\phi_f(\mathbf{x}) \langle b|\phi_f\rangle \langle\phi_f|\hat{S}|\phi_i\rangle \langle\phi_i|a\rangle. \quad (2.8)$$

Upon explicitly extracting the time dependence from the annihilation operators in (2.8) and (2.6) by writing  $a_{\mathbf{k}} \rightarrow a_{\mathbf{k}} e^{-i\omega_{\mathbf{k}}T_i}$  and  $b_{\mathbf{k}}^* \rightarrow b_{\mathbf{k}}^* e^{i\omega_{\mathbf{k}}T_f}$ , and using the functional integral representation of  $\langle\phi_f|\hat{S}|\phi_i\rangle$ , one can write

$$S(b^*, a) = \int \mathcal{D}\phi(x) \exp\left[iS[\phi] + B_i(\phi_i, a) + B_f(\phi_f, b^*)\right], \quad (2.9)$$

where the integral over the boundary configurations  $\phi_i$  and  $\phi_f$  and the integral over all paths interpolating between these configurations have been combined into a single path integral, and the boundary terms are given by

$$B_i(\phi_i, a) = \int d^3k \left\{ -\frac{1}{2} a_{\mathbf{k}} a_{-\mathbf{k}} e^{-2i\omega_{\mathbf{k}} T_i} - \frac{1}{2} \omega_{\mathbf{k}} \phi_i(\mathbf{k}) \phi_i(-\mathbf{k}) + \sqrt{2\omega_{\mathbf{k}}} a_{\mathbf{k}} e^{-i\omega_{\mathbf{k}} T_i} \phi_i(\mathbf{k}) \right\} \quad (2.10a)$$

$$B_f(\phi_f, b^*) = \int d^3k \left\{ -\frac{1}{2} b_{\mathbf{k}}^* b_{-\mathbf{k}}^* e^{2i\omega_{\mathbf{k}} T_f} - \frac{1}{2} \omega_{\mathbf{k}} \phi_f(\mathbf{k}) \phi_f(-\mathbf{k}) + \sqrt{2\omega_{\mathbf{k}}} b_{\mathbf{k}}^* e^{i\omega_{\mathbf{k}} T_f} \phi_f(-\mathbf{k}) \right\} . \quad (2.10b)$$

To proceed, the sums over initial and final states in (2.1) are replaced by

$$\sum_i \rightarrow \int \mathcal{D}a_{\mathbf{k}}^* \mathcal{D}a_{\mathbf{k}} \exp \left[ - \int d^3k a_{\mathbf{k}}^* a_{\mathbf{k}} \right] \quad (2.11a)$$

$$\sum_f \rightarrow \int \mathcal{D}b_{\mathbf{k}}^* \mathcal{D}b_{\mathbf{k}} \exp \left[ - \int d^3k b_{\mathbf{k}}^* b_{\mathbf{k}} \right] , \quad (2.11b)$$

and unity, in the form

$$\int \mathcal{D}c_{\mathbf{k}}^* \mathcal{D}c_{\mathbf{k}} \exp \left[ - \int d^3k c_{\mathbf{k}}^* c_{\mathbf{k}} \right] |c\rangle \langle c| = \mathbf{1} , \quad (2.12)$$

is inserted between  $\hat{S}$  and  $\hat{P}_E \hat{P}_N$ , giving

$$\begin{aligned} \sigma(E, N) &= \int \mathcal{D}[a, b, c, e] \exp [-b^* b - a^* a - c^* c - e^* e] \quad (2.13) \\ &S(b^*, c) S(b^*, e)^* \langle c | \hat{P}_E \hat{P}_N | a \rangle \langle a | \hat{P}_E \hat{P}_N | e \rangle . \end{aligned}$$

We are using an obvious short-hand notation for the integration measure, and integrals over momenta are implied. The kernels of the projection operators take the form

$$\langle b | \hat{P}_E | a \rangle = \int d\xi \exp \left[ -iE\xi + \int d^3k e^{i\omega_{\mathbf{k}} \xi} b_{\mathbf{k}}^* a_{\mathbf{k}} \right] \quad (2.14a)$$

$$\langle b | \hat{P}_N | a \rangle = \int d\eta \exp \left[ -iN\eta + \int d^3k e^{i\eta} b_{\mathbf{k}}^* a_{\mathbf{k}} \right] , \quad (2.14b)$$

from which it follows that

$$\langle b | \hat{P}_E \hat{P}_N | a \rangle = \int d\xi d\eta \exp \left[ -iE\xi - iN\eta + \int d^3k e^{i\omega_{\mathbf{k}} \xi + i\eta} b_{\mathbf{k}}^* a_{\mathbf{k}} \right] . \quad (2.15)$$

After substituting (2.9) and (2.15) into (2.13), and then changing variables via  $a \rightarrow \exp[-i\omega\xi - i\eta] a$  and  $a^* \rightarrow \exp[-i\omega\xi' - i\eta'] a^*$ , the  $c$ -integral may be performed to obtain

$$\int \mathcal{D}c^* \mathcal{D}c \exp \left[ -c^*c + c^*a + B_i(\phi_i, c) \right] = \exp[B_i(\phi_i, a)] , \quad (2.16)$$

with a similar expression for the  $e$ -integration. Finally, after collecting terms and redefining  $\xi + \xi' \rightarrow \xi$  and  $\eta + \eta' \rightarrow \eta$ , the cross section becomes

$$\sigma(E, N) = \int \mathcal{D}\phi(x) \mathcal{D}\phi'(x) \mathcal{D}a_{\mathbf{k}}^* \mathcal{D}a_{\mathbf{k}} \mathcal{D}b_{\mathbf{k}}^* \mathcal{D}b_{\mathbf{k}} d\eta d\xi \exp[W] , \quad (2.17a)$$

where

$$\begin{aligned} W = & -iE\xi - iN\eta - \int d^3k \left\{ b_{\mathbf{k}}^* b_{\mathbf{k}} + a_{\mathbf{k}}^* a_{\mathbf{k}} e^{-i\Delta_{\mathbf{k}}} \right\} \\ & + iS[\phi] - iS[\phi'] + B_i(\phi_i, a) + B_f(\phi_f, b^*) + B_i(\phi'_i, a)^* + B_f(\phi'_f, b^*)^* , \end{aligned} \quad (2.17b)$$

with  $\Delta_{\mathbf{k}} = \omega_{\mathbf{k}}\xi + \eta$ . The functional  $S[\phi(x)]$  is the action, and the boundary terms at the initial and final times  $T_i$  and  $T_f$  are given by (2.10).

To display the semiclassical nature of the cross section, it is convenient to express the exponential factor  $W$  in terms of the rescaled field  $\tilde{\phi} = g\phi$ , the rescaled mode amplitudes  $\tilde{a}_{\mathbf{k}} = g a_{\mathbf{k}}$  and  $\tilde{b}_{\mathbf{k}} = g b_{\mathbf{k}}$ , and the rescaled energy  $\epsilon$  and particle number  $\nu$  defined in (2.2). The action  $\tilde{S}[\tilde{\phi}]$ , which is related to the unscaled action by  $S[\phi] = \tilde{S}[\tilde{\phi}]/g^2$ , is  $g$ -independent and we can thus write  $W(E, N) = F(\epsilon, \nu)/g^2$ , with the function  $F$  being independent of the coupling constant. Hence, for small values of  $g$ , it is a good approximation to simply saturate the integrals by classical saddle-point solutions, from which we obtain

$$\sigma(E, N) = \exp \left[ \frac{1}{g^2} F(\epsilon, \nu) \right] , \quad (2.18)$$

where  $F$  is determined by evaluating (2.17b) on the classical solution. In what follows we shall work only with the rescaled quantities in which the  $g$ -dependence has been factored out, but for notational simplicity we will use the unscaled notation and drop the tilde over the associated quantity.

In looking for saddle-points of (2.17b) we must distinguish between two cases. There may be solutions which correspond to classically allowed evolution, in which case the fields and the action will be real and the parameter  $\Delta_{\mathbf{k}}$  zero. As shown below, this implies that the function  $F$  of (2.18) will be zero, signalling the absence of suppression, and if we can find such classical solutions with small  $\nu$ , this furthermore indicates that the two-particle rates are likewise unsuppressed. Classically allowed evolution which changes the topology of the fields must perforce occur at an energy above the sphaleron barrier, but  $E > E_{\text{sph}}$  is per se not a sufficient condition for the existence of classically allowed solutions with a given particle number in the initial state, and in a later section we shall return to the problem of finding topology changing solutions with low incident particle number.

Alternatively, there may be solutions which correspond to classically forbidden processes, in which case the saddle-points for  $\phi$  and  $\phi'$ ,  $\delta S[\phi]/\delta\phi = 0$  and  $\delta S[\phi']/\delta\phi' = 0$ , may in fact have imaginary components, while the saddle-point values of  $a$  and  $a^*$  need not be complex conjugates. Obtaining these complexified saddle-points is much more involved than finding classically allowed solutions passing over the sphaleron barrier, and so we devote the remainder of this section to explicating some of the details of the procedure, with a special emphasis on boundary conditions.

Extremizing (2.17b) with respect to modes  $a_{\mathbf{k}}$  and  $a_{\mathbf{k}}^*$  yields

$$a_{\mathbf{k}}^* e^{-i\Delta_{\mathbf{k}}} + a_{-\mathbf{k}} e^{-2i\omega T_i} - \sqrt{2\omega} \phi_i(\mathbf{k}) e^{-i\omega T_i} = 0 \quad (2.19a)$$

$$a_{\mathbf{k}} e^{-i\Delta_{\mathbf{k}}} + a_{-\mathbf{k}}^* e^{2i\omega T_i} - \sqrt{2\omega} \phi'_i(-\mathbf{k}) e^{i\omega T_i} = 0 , \quad (2.19b)$$

which may be solved to give the saddle-points

$$a_{\mathbf{k}} = \frac{\sqrt{2\omega_{\mathbf{k}}}}{e^{-i\Delta_{\mathbf{k}}} - e^{i\Delta_{\mathbf{k}}}} \left[ \phi'_i(-\mathbf{k}) - e^{i\Delta_{\mathbf{k}}} \phi_i(-\mathbf{k}) \right] e^{i\omega_{\mathbf{k}} T_i} \quad (2.20a)$$

$$\bar{a}_{\mathbf{k}} = \frac{\sqrt{2\omega_{\mathbf{k}}}}{e^{-i\Delta_{\mathbf{k}}} - e^{i\Delta_{\mathbf{k}}}} \left[ \phi_i(\mathbf{k}) - e^{i\Delta_{\mathbf{k}}} \phi'_i(\mathbf{k}) \right] e^{-i\omega_{\mathbf{k}} T_i} . \quad (2.20b)$$

As previously noted, in general these solutions are not complex conjugates, and hence we use the bar notation for the latter. The expression (2.20) relates the  $a$ -mode amplitudes to the initial saddle-point values of the incident fields, which in turn are constrained by

$$-i\dot{\phi}_i(\mathbf{k}) - \omega\phi_i(\mathbf{k}) + \sqrt{2\omega} a_{-\mathbf{k}} e^{-i\omega T_i} = 0 \quad (2.21a)$$

$$i\dot{\phi}'_i(\mathbf{k}) - \omega\phi'_i(\mathbf{k}) + \sqrt{2\omega} a_{\mathbf{k}}^* e^{i\omega T_i} = 0 , \quad (2.21b)$$

and with the use of (2.20), one can write this expression as a boundary condition involving only the incident fields,

$$i\dot{\phi}_i(\mathbf{k}) + \omega\phi_i(\mathbf{k}) = e^{i\Delta_{\mathbf{k}}} \left[ i\dot{\phi}'_i(\mathbf{k}) + \omega\phi'_i(\mathbf{k}) \right] \quad (2.22a)$$

$$i\dot{\phi}_i(\mathbf{k}) - \omega\phi_i(\mathbf{k}) = e^{-i\Delta_{\mathbf{k}}} \left[ i\dot{\phi}'_i(\mathbf{k}) - \omega\phi'_i(\mathbf{k}) \right] . \quad (2.22b)$$

The parameter  $\Delta_{\mathbf{k}}$  itself is determined by saddle-point equations, and when it vanishes note that  $\phi'_i(\mathbf{k}) = \phi_i(\mathbf{k})$ , and that  $a_{\mathbf{k}} = (\omega_{\mathbf{k}}/2)^{1/2} \phi_i(-\mathbf{k}) e^{i\omega_{\mathbf{k}} T_i}$  and  $\bar{a}_{\mathbf{k}} = (\omega_{\mathbf{k}}/2)^{1/2} \phi_i(\mathbf{k}) e^{-i\omega_{\mathbf{k}} T_i}$  are complex conjugates. This case therefore corresponds to a classically allowed process above the sphaleron barrier.

To obtain final-state boundary conditions, one extremises (2.17b) with respect to the  $b$ -modes and the final-state fields  $\phi_f$  and  $\phi'_f$ , which gives

$$b_{\mathbf{k}}^* + b_{-\mathbf{k}} e^{-2i\omega T_f} - \sqrt{2\omega} \phi'_f(\mathbf{k}) e^{-i\omega T_f} = 0 \quad (2.23a)$$

$$b_{\mathbf{k}} + b_{-\mathbf{k}}^* e^{2i\omega T_f} - \sqrt{2\omega} \phi_f(-\mathbf{k}) e^{i\omega T_f} = 0 , \quad (2.23b)$$

and

$$i\dot{\phi}_f(\mathbf{k}) - \omega\phi_f(\mathbf{k}) + \sqrt{2\omega} b_{\mathbf{k}}^* e^{i\omega T_f} = 0 \quad (2.24a)$$

$$-i\dot{\phi}'_f(\mathbf{k}) - \omega\phi'_f(\mathbf{k}) + \sqrt{2\omega} b_{-\mathbf{k}} e^{-i\omega T_f} = 0 . \quad (2.24b)$$

Together, (2.23) and (2.24) imply that the final-state fields and their respective time derivatives agree,  $\phi'_f(\mathbf{k}) = \phi_f(\mathbf{k})$  and  $\dot{\phi}'_f(\mathbf{k}) = \dot{\phi}_f(\mathbf{k})$ . Thus, as the saddle-points  $\phi$

and  $\phi'$  satisfy the same classical equations at intermediate times, they also agree at these times, and hence we are really dealing with a single solution  $\phi(x)$ . At first sight this seems inconsistent with (2.22) for nonzero  $\Delta_{\mathbf{k}}$ . However, the general complex saddle-point solution is nonanalytic, and  $\phi_i$  and  $\phi'_i$  in (2.22) are to be thought of as lying on separate sheets in the complex- $t$  plane (to emphasize this, we will not remove the prime from  $\phi'_i$ ).

The value of  $\Delta_{\mathbf{k}}$  is determined by the saddle-points of  $\xi$  and  $\eta$ , which from (2.17b) are related to the energy and particle number by

$$\epsilon = \int d^3k \omega_{\mathbf{k}} a_{\mathbf{k}}^* a_{\mathbf{k}} e^{-i\Delta_{\mathbf{k}}} \quad (2.25a)$$

$$\nu = \int d^3k a_{\mathbf{k}}^* a_{\mathbf{k}} e^{-i\Delta_{\mathbf{k}}} . \quad (2.25b)$$

The saddle-point of  $\xi$  may be made pure imaginary by a suitable time-translation, and the real part of the  $\eta$ -saddle-point is typically small [11], so we can write

$$\xi = iT \quad (2.26a)$$

$$\eta = i\theta . \quad (2.26b)$$

The parameter  $T$  can be removed from the boundary conditions by choosing the complex time contours of Fig. 1. Since the fields become linear in the distant past we can write

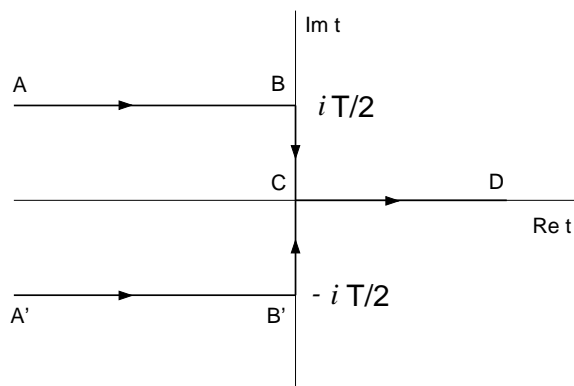


FIG. 1. Complex-time contours

$$\phi(\mathbf{k}) = \frac{1}{\sqrt{2\omega_{\mathbf{k}}}} \left[ f_{\mathbf{k}} e^{-i\omega_{\mathbf{k}}\tau} + g_{\mathbf{k}} e^{i\omega_{\mathbf{k}}\tau} \right] \quad \text{on line AB} \quad (2.27a)$$

$$\phi'(\mathbf{k}) = \frac{1}{\sqrt{2\omega_{\mathbf{k}}}} \left[ f'_{\mathbf{k}} e^{-i\omega_{\mathbf{k}}\tau} + g'_{\mathbf{k}} e^{i\omega_{\mathbf{k}}\tau} \right] \quad \text{on line A'B'} \quad (2.27b)$$

as  $\tau = \text{Re } t \rightarrow -\infty$ . The boundary conditions (2.22) will be applied along line  $AB$ , keeping in mind that  $\phi_i$  and  $\phi'_i$  lie on different sheets in this region. In this asymptotic linear domain, however, the fields are analytic on their respective sheets, and hence

$$\phi'(\mathbf{k}) = \frac{1}{\sqrt{2\omega_{\mathbf{k}}}} \left[ f'_{\mathbf{k}} e^{\omega T - i\omega_{\mathbf{k}}\tau} + g'_{\mathbf{k}} e^{-\omega T + i\omega_{\mathbf{k}}\tau} \right] \quad \text{on line AB} \quad (2.28)$$

as  $\tau \rightarrow -\infty$ . This relation, with (2.27a) and boundary conditions (2.22), gives the restriction

$$f'_{\mathbf{k}} = e^{\theta} f_{\mathbf{k}} \quad (2.29a)$$

$$g'_{\mathbf{k}} = e^{-\theta} g_{\mathbf{k}} , \quad (2.29b)$$

and the degrees of freedom associated with the field along  $A'B'$  have been eliminated.

A number of simplifications now occur. The energy and particle number may be written

$$\epsilon = \int d^3k \omega_{\mathbf{k}} f_{\mathbf{k}}^* g_{-\mathbf{k}} \quad (2.30a)$$

$$\nu = \int d^3k f_{\mathbf{k}}^* g_{-\mathbf{k}} . \quad (2.30b)$$

Upon taking the limits  $T_i \rightarrow -\infty$  and  $T_f \rightarrow \infty$  the boundary terms become

$$B_i(\phi_i, a) = B_i^*(\phi'_i, a) = \frac{1}{2} \int d^3k f_{-\mathbf{k}} g_{\mathbf{k}} \quad (2.31a)$$

$$B_f(\phi_f, b^*) = B_f^*(\phi'_f, b^*) = \frac{1}{2} \int d^3k b_{\mathbf{k}}^* b_{\mathbf{k}} , \quad (2.31b)$$

and thus the exponential factor on the solution takes the form

$$F = \epsilon T + \nu \theta + iS[\phi] - iS[\phi'] , \quad (2.32)$$

where the (rescaled  $g$ -independent) actions  $S[\phi]$  and  $S[\phi']$  are evaluated along the upper contour  $ABCD$  on the first and second sheets respectively.

By virtue of a symmetry akin to  $CPT$ , these expressions simplify considerably if the saddle-point is unique. Since the coefficients of the field equations  $\delta S[\phi]/\delta\phi = 0$  are real, given a solution  $\phi(\mathbf{x}, t)$ , one can form a new solution  $\Phi(\mathbf{x}, t) = \phi(\mathbf{x}, t^*)^*$ . Uniqueness then implies the conjugation symmetry  $\phi(\mathbf{x}, t) = \phi(\mathbf{x}, t^*)^*$ , and hence  $f'_{\mathbf{k}} = g^*_{-\mathbf{k}}$  and  $g'_{\mathbf{k}} = f^*_{-\mathbf{k}}$ . This can be used to express (2.29) as

$$g_{\mathbf{k}} = e^{\theta} f^*_{-\mathbf{k}} , \quad (2.33)$$

from which it follows that the energy and particle number take the form

$$\epsilon = e^{-\theta} \int d^3k \omega_{\mathbf{k}} f_{\mathbf{k}}^* f_{\mathbf{k}} \quad (2.34a)$$

$$\nu = e^{-\theta} \int d^3k f_{\mathbf{k}}^* f_{\mathbf{k}} . \quad (2.34b)$$

Expression (2.33) may also be used to rewrite the boundary conditions (2.27) in the rather convenient form

$$\phi(\mathbf{k}) = \frac{1}{\sqrt{2\omega_{\mathbf{k}}}} \left[ f_{\mathbf{k}} e^{-i\omega_{\mathbf{k}}\tau} + e^{\theta} f_{\mathbf{k}}^* e^{i\omega_{\mathbf{k}}\tau} \right] \quad \text{on line AB} \quad (2.35a)$$

$$\phi'(\mathbf{k}) = \frac{1}{\sqrt{2\omega_{\mathbf{k}}}} \left[ e^{\theta} f_{\mathbf{k}} e^{-i\omega_{\mathbf{k}}\tau} + f_{\mathbf{k}}^* e^{i\omega_{\mathbf{k}}\tau} \right] \quad \text{on line A'B'} \quad (2.35b)$$

as  $\tau \rightarrow -\infty$ . Note that the conjugation symmetry implies that the solution is real along the entire real-Minkowski axis, and we shall thus impose the additional boundary condition  $\text{Im} \phi(\mathbf{x}, t = 0) = 0$ . In general, however, the solution becomes complex along the time-contours  $ABC$  and  $A'B'C$ , and the consistency of (2.35a) and (2.35b) requires that  $\phi(x)$  also possesses singularities between these contours. For the case in which  $\theta = 0$ , the field becomes real along  $AB$  and  $A'B'$  in the infinite past, and hence it remains real along the entire upper and lower contours. When the solution

is also real along the imaginary-time axis, as is the case for periodic instantons [9], turning-point boundary conditions  $\dot{\phi} = 0$  are also satisfied at  $B$ ,  $B'$  and  $C$ .

Recall that in (2.32), both  $S = S[\phi]$  and  $S' = S[\phi']$  are evaluated along the contour  $ABCD$ , albeit on different sheets in the complex- $t$  plane. If the singularities of  $\phi$  only lie between  $AB$  and  $A'B'$ , the action  $S'$  along  $ABCD$  is equal to the action along  $A'B'CD$  (staying on the same sheet, and assuming no contribution from the contour at infinity). Hence, the conjugation symmetry implies  $S' = S^*$ , and thus

$$F = \epsilon T + \nu\theta - 2 \operatorname{Im} S(T, \theta) , \quad (2.36)$$

where the implicit  $T$  and  $\theta$  dependence in the action has been made explicit. Note that  $S(T, \theta)$  can be obtained by integrating only along  $ABC$ , as the contribution from the Minkowski section  $CD$  is real and does not contribute to  $F$ . Furthermore, since  $T$  and  $\theta$  (or equivalently  $\xi$  and  $\eta$ ) are determined by the saddle-point of  $F$ , we have

$$\epsilon = 2 \operatorname{Im} \frac{\partial \tilde{S}}{\partial T} \quad (2.37a)$$

$$\nu = 2 \operatorname{Im} \frac{\partial \tilde{S}}{\partial \theta} , \quad (2.37b)$$

an alternate expression for the energy and particle number that can be used as a consistency check.

In this section we have presented the formalism of Rubakov, Son, and Tinyakov [4] in some detail. The case of a single real scalar field has been used for purposes of illustration only, and the method is easily extended to more complicated theories. In most instances, and in particular for the standard model, the relevant saddle-point solutions must be obtained computationally. The function  $F(\epsilon, \nu)$  can then be determined, and the cross section (2.18) calculated. Finding these complexified saddle-points, however, is a formidable numerical challenge, and in the next subsection we outline some of our progress towards this goal and we present a few initial results.

### C. Some Initial Computational Results

Together with Peter Tinyakov, we are presently engaged in the formidable numerical task of finding the Euclidean-Minkowski hybrid solutions and extracting the baryon number violating cross sections. Our approach in the classically forbidden regime is to map the constant  $F$ -contours by exploring the two parameter family of solutions determined by  $\theta$  and  $T$ . As this investigation has just begun, we shall only present some preliminary results and briefly discuss our future plans. The numerical approach in the classically allowed domain above the sphaleron barrier is quite different and involves exploring the  $\epsilon$ - $\nu$  plane using Monte Carlo sampling techniques, and we shall present the details of this separate investigation in the next section.

As previously stated, we are considering the standard model with the Weinberg angle set to zero. The resulting spontaneously broken  $SU(2)$  gauge theory possesses all the relevant physics while undergoing notable simplification. The action for the bosonic sector of this theory is

$$S = \int dx^4 \left\{ -\frac{1}{2} \text{Tr} F_{\mu\nu} F^{\mu\nu} + D_\mu \Phi^\dagger D^\mu \Phi - \lambda (\Phi^\dagger \Phi - 1)^2 \right\}, \quad (2.38)$$

where the indices run from 0 to 3 and where

$$F_{\mu\nu} = \partial_\mu A_\nu - \partial_\nu A_\mu - i[A_\mu, A_\nu] \quad (2.39)$$

$$D_\mu \Phi = (\partial_\mu - iA_\mu) \Phi. \quad (2.40)$$

We use the standard metric  $\eta = \text{diag}(1, -1, -1, -1)$ , and have eliminated several constants by a suitable choice of units. We have also set  $g = 1$ , but when needed we shall restore the gauge coupling to its physical value of  $g = 0.652$ . For our numerical work we take  $\lambda = 0.1$ , which corresponds to a Higgs mass of about  $M_H = 72 \text{ GeV}$ .

To yield a computationally manageable system, we work in the spherical *Ansatz* of Ref. [15] in which the gauge and Higgs fields are parameterized in terms of six real functions  $a_0, a_1, \alpha, \beta, \mu, \nu$  of  $r$  and  $t$ :

$$A_0(\mathbf{x}, t) = \frac{1}{2} a_0(r, t) \boldsymbol{\sigma} \cdot \hat{\mathbf{x}} \quad (2.41a)$$

$$A_i(\mathbf{x}, t) = \frac{1}{2} \left[ a_1(r, t) \boldsymbol{\sigma} \cdot \hat{\mathbf{x}} \hat{x}^i + \frac{\alpha(r, t)}{r} (\sigma^i - \boldsymbol{\sigma} \cdot \hat{\mathbf{x}} \hat{x}^i) + \frac{1 + \beta(r, t)}{r} \epsilon^{ijk} \hat{x}^j \sigma^k \right] \quad (2.41b)$$

$$\Phi(\mathbf{x}, t) = [\mu(r, t) + i\nu(r, t) \boldsymbol{\sigma} \cdot \hat{\mathbf{x}}] \hat{\xi} \quad (2.41c)$$

where  $\hat{\mathbf{x}}$  is the unit three-vector in the radial direction and  $\hat{\xi}$  is an arbitrary two-component complex unit-vector. For the 4-dimensional fields to be regular at the origin,  $a_0$ ,  $\alpha$ ,  $a_1 - \alpha/r$ ,  $(1 + \beta)/r$  and  $\nu$  must vanish like some appropriate power of  $r$  as  $r \rightarrow 0$ .

These spherical configurations reduce the system to an effective 1+1 dimensional theory on the spatial half-line. The action of the reduced system follows by inserting (2.41) into (2.38), and after some algebra one obtains [15]

$$S = 4\pi \int dt \int_0^\infty dr \left[ -\frac{1}{4} r^2 f^{\mu\nu} f_{\mu\nu} + D^\mu \chi^* D_\mu \chi + r^2 D^\mu \phi^* D_\mu \phi - \frac{1}{2r^2} (|\chi|^2 - 1)^2 - \frac{1}{2} (|\chi|^2 + 1) |\phi|^2 - \text{Re}(i\chi^* \phi^2) - \lambda r^2 (|\phi|^2 - 1)^2 \right], \quad (2.42)$$

where the indices now run from 0 to 1 and are raised and lowered with  $\eta_{\mu\nu} = \text{diag}(1, -1)$ , and where

$$f_{\mu\nu} = \partial_\mu a_\nu - \partial_\nu a_\mu \quad (2.43a)$$

$$\chi = \alpha + i\beta \quad (2.43b)$$

$$\phi = \mu + i\nu \quad (2.43c)$$

$$D_\mu \chi = (\partial_\mu - i a_\mu) \chi \quad (2.43d)$$

$$D_\mu \phi = \left( \partial_\mu - \frac{i}{2} a_\mu \right) \phi. \quad (2.43e)$$

This is an effective 2-dimensional  $U(1)$  gauge theory spontaneously broken by two scalar fields. It possesses the same rich topological structure as the full 4-dimensional theory and provides an excellent testing ground for numerical exploration.

In the rest of this section, we examine spherically symmetry Euclidean-Minkowski solutions lying on the  $ABCD$  time-contour of Fig. 1, satisfying the aforementioned boundary conditions. In particular, the real gauge field  $a_\mu$  becomes complex and obeys the boundary condition

$$a_\mu(k) = g_{\mu,k} e^{-i\omega_k\tau} + e^\theta g_{\mu,k}^* e^{i\omega_k\tau} \quad \text{on AB as } \tau = \text{Re } t \rightarrow -\infty, \quad (2.44)$$

where we have absorbed the factor involving  $\omega_k$  into the definition of the amplitudes. For each value of the space-time index  $\mu$ , we are thus searching for two independent real degrees of freedom (as the saddle-point solution  $a_\mu$  is complex). The real and the imaginary components of the complex fields  $\chi$  and  $\phi$  may be treated in a similar manner, giving a total of four real degrees of freedom for each field. We are thus looking for two independent complex fields  $\chi$  and  $\bar{\chi}$ , with boundary conditions

$$\begin{aligned} \chi(k) &= f_k e^{-i\omega_k\tau} + e^\theta h_k e^{i\omega_k\tau} \\ \bar{\chi}(k) &= h_k^* e^{-i\omega_k\tau} + e^\theta f_k^* e^{i\omega_k\tau} \quad \text{on AB as } \tau \rightarrow -\infty, \end{aligned} \quad (2.45)$$

and for two complex fields  $\phi$  and  $\bar{\phi}$  with similar boundary conditions. When  $\theta = 0$ , the solution becomes “real” along the entire  $ABCD$  contour, in the sense that  $a_\mu$  is real, while  $\bar{\chi} = \chi^*$  and  $\bar{\phi} = \phi^*$ .

In a future publication we plan to numerically find these solutions and to explore the behavior of the suppression function  $F(\epsilon, \nu)$  throughout much of the  $\epsilon$ - $\nu$  plane. In this paper, however, we restrict ourselves to the periodic instantons of Ref. [9] for which  $\theta = 0$ .

As path  $EF$  of Fig. 2 illustrates, zero energy instantons are Euclidean solutions that interpolate between consecutive vacua. In contrast, periodic instantons are Euclidean solutions that interpolate between configurations of nonzero energy lying in adjacent topological sectors, as in path  $E'F'$  of Fig. 2. They have nonzero energy,

finite periods, and possess turning points (located at  $E'$  and  $F'$  in the Figure). Given a periodic instanton, we may choose the parameter  $T$  of Fig. 1 to coincide with the corresponding period, and hence we may take  $C$  and  $B$  to be the turning points  $E'$  and  $F'$  (with a time separation of  $iT/2$ ).

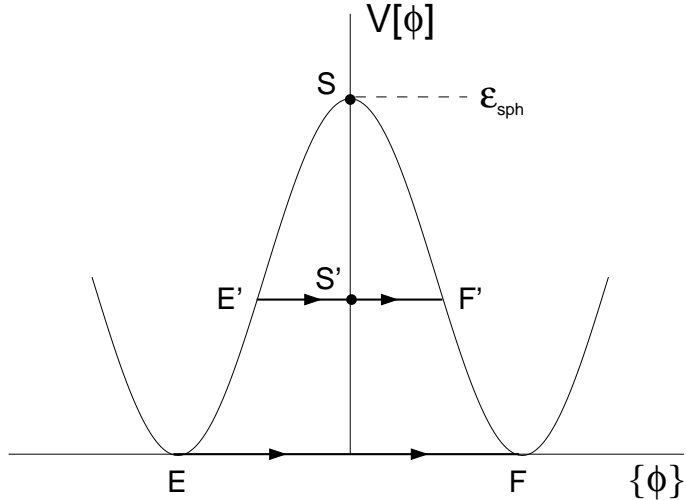


FIG. 2. The instanton ( $EF$ ), the sphaleron ( $S$ ), and the periodic instanton ( $E'F'$ ). The horizontal axis represents the infinite dimensional field space, and the vertical axis marks the potential energy of a corresponding field configuration.

We now wish to numerically find the periodic instanton along the imaginary time axis. These solutions are real along the Euclidean axis, in the sense that  $a_\mu$  is real, while  $\bar{\chi} = \chi^*$  and  $\bar{\phi} = \phi^*$ . Moreover, since the time derivatives vanish at  $B$  and  $C$ , the periodic instanton remains real when continued both to the real axis and to the contour  $AB$  (consistent with the vanishing of  $\theta$ ).

While finding these solutions is less challenging than obtaining the general saddlepoints with nonzero  $\theta$ , we must still resort to computational methods. However, before describing our numerical approach, it is useful to examine two instances in which  $F$  can be found analytically. Both the usual zero energy instanton and the sphaleron can be viewed as limiting cases of periodic instantons, and they are illustrated in Fig. 2. The instanton represents a vacuum-to-vacuum tunneling event, and as such

lies at the origin of the  $\epsilon$ - $\nu$  plane, thus giving  $F(0, 0) = -2 \text{Im } S_{\text{inst}} = -16\pi^2$ . The sphaleron, on the other hand, has both nonzero energy and particle number,  $\epsilon_{\text{sph}}$  and  $\nu_{\text{sph}}$  respectively <sup>†</sup>. It is analytic over the entire complex- $t$  plane, with a contribution to  $\text{Im } S$  only along  $BC$  in Fig. 1, and hence  $F(\epsilon_{\text{sph}}, \nu_{\text{sph}}) = \epsilon_{\text{sph}}T - 2 \text{Im } S_{\text{sph}} = 0$ .

We now have the value of  $F$  at two key points in the  $\epsilon$ - $\nu$  plane. The former gives the usual low energy 't Hooft suppression of the baryon number violation rates, while the latter yields unsuppressed rates at the sphaleron energy, albeit for very large incident particle number (as in a thermal plasma in the early universe). All other periodic instantons lie along a line connecting these two points, and  $F$  monotonically increases from  $-16\pi^2$  to zero as we traverse this line from the origin to the sphaleron. We now concentrate on finding these solutions and their corresponding values of  $F$ .

It is convenient to work in the  $a_0 = 0$  gauge, and to shift the zero of time so that turning points  $C$  and  $B$  are located at  $t = -iT/4$  and  $t = iT/4$ , respectively. That is to say,

$$\dot{\chi}(r, iT/4) = 0 \tag{2.46a}$$

$$\dot{\phi}(r, iT/4) = 0 \tag{2.46b}$$

$$\dot{a}_1(r, iT/4) = 0, \tag{2.46c}$$

with vanishing time derivatives also at  $t = -iT/4$ . Since the fields merely retrace their steps after the turning points, it is sufficient to find the periodic instanton only over the half-period from  $t = -iT/4$  and  $t = iT/4$  between consecutive turning points,

---

<sup>†</sup>Technically, since the sphaleron is a static nonlinear configuration, it does not have a particle number; however, a gently perturbed sphaleron will decay into a state with a well defined particle number  $\nu_{\text{sph}}$ . It is the decaying sphaleron, or rather the time reversed solution, that we are actually speaking of here. To give a feeling for the numbers involved, when  $g = 1$  and  $\lambda = 0.1$ , the sphaleron energy is  $\epsilon_{\text{sph}} = 2.5447$  and the asymptotic particle number is  $\nu_{\text{sph}} = 1.7478$  (in physical units with  $g = 0.065$ ,  $E_{\text{sph}} \sim 10 \text{ TeV}$  and  $N_{\text{sph}} \sim 50$ ).

which will considerably reduce our computational effort. In fact, we can be even more economical by exploiting an additional symmetry akin to time invariance, and it will then suffice to find the periodic instanton only over the quarter period, from  $t = 0$  to  $t = iT/4$ .

For any solution  $\chi(r, t)$ ,  $\phi(r, t)$ , and  $a_1(r, t)$  to the classical equations of motion, we may construct another solution given by

$$\chi'(r, t) = -\chi^*(r, -t) \quad (2.47a)$$

$$\phi'(r, t) = -\phi^*(r, -t) \quad (2.47b)$$

$$a_1'(r, t) = -a_1(r, -t) . \quad (2.47c)$$

This can be traced to a combination of parity symmetry (in the full 4-dimensional theory),  $\phi \rightarrow -\phi$  invariance, and simple time reflection  $t \rightarrow -t$ . In terms of the reduced theory, this is none other than the 2-dimensional time reversed solution (which should not be confused with 4-dimensional time reversal).

A corresponding time reversed solution may be obtained from any given solution by appropriately changing the initial conditions in a manner dictated by (2.47).

However, if the initial conditions take the form,

$$\chi(r, 0) = \text{imaginary} \quad \dot{\chi}(r, 0) = \text{real} \quad (2.48a)$$

$$\phi(r, 0) = \text{imaginary} \quad \dot{\phi}(r, 0) = \text{real} \quad (2.48b)$$

$$a_1(r, 0) = 0 , \quad (2.48c)$$

(with no restriction on the time derivative of  $a_1$ ), then the solution will be invariant under time reversal:  $\chi' = \chi$ ,  $\phi' = \phi$ , and  $a_1' = a_1$ , i.e.

$$\chi(r, -t) = -\chi^*(r, t) \quad (2.49a)$$

$$\phi(r, -t) = -\phi^*(r, t) \quad (2.49b)$$

$$a_1(r, -t) = -a_1(r, t) , \quad (2.49c)$$

and in this case, we only need to look for solutions over the quarter period from  $t = 0$  to  $t = iT/4$ , satisfying the initial and final conditions (2.46) and (2.48).

We must also choose boundary conditions at the origin and spatial infinity in such a way as to ensure regularity of the corresponding 4-dimensional fields. For the  $\chi$  field, we must take  $\chi(0, t) = -i$ , and we may choose a gauge in which  $\chi(r, t) = i$  as  $r \rightarrow \infty$ . Thus, as the initial  $\chi$ -configuration is pure imaginary, it will always have a zero for some nonzero value of  $r$ . As will be discussed more thoroughly in the next section, the sphaleron is a spherical configuration with vanishing  $a_\mu$  and with pure imaginary  $\chi$  and  $\phi$ ; furthermore, like the initial configuration, its  $\chi$ -field possesses a zero at some radius  $r$  away from the origin. Hence, the initial configurations (2.48) will not lie far from the sphaleron, as indicated by the close proximity of  $S'$  and  $S$  in Fig. 2.

To find the periodic instanton numerically, we place the system in a box of spatial extent  $L_r$  and time extent  $L_t$ , and then discretize the action (2.42) using the standard techniques of lattice gauge theory. The space-time grid has lattice sites at  $(i\Delta r, j\Delta t)$ , where  $i = 0 \cdots N_r$  and  $j = 0 \cdots N_t$ . The fields  $\chi$  and  $\phi$  become discrete variables defined on these sites, while  $a_1$  is defined on the space-links and time-sites (in a gauge where  $a_0$  does not vanish, it is defined on the space-sites and time-links). We take  $N_r = 64$ ,  $N_t = 40$ , with  $dr = 0.05$ , and impose (2.46) and (2.48) on the lower and upper time slices  $j = 0$  and  $j = N_t$  respectively. The parameter  $\Delta t$ , which is taken between 0.02 to 0.04, controls the period of the periodic instanton through  $T = 4\Delta t N_t$ .

Starting from an initial guesses along the Euclidean axis satisfying the appropriate boundary conditions, we search for a minimum of the action using the method of conjugate gradients. Like the naive gradient descent, the conjugate gradient algorithm chooses its descent direction based upon the gradient. A new guess is then selected

lying further down the slope, and the algorithm is repeated. With each new iteration, the configuration finds itself closer and closer to the local minimum, and eventually one can approximate the extremum to within the desired tolerance. The advantage of the conjugate gradient method over a simple gradient descent, is that the former achieves a much more rapid convergence rate by judiciously shifting the direction of descent slightly away from the gradient. As this method is rather standard, we shall not describe it in any more detail.

A straightforward application of the algorithm, however, yields little success. Periodic instanton may be found in this manner, but unless one starts extremely close to a solution, one typically relaxes to the static sphaleron. The two turning points of the initial guess,  $E'$  and  $F'$  in Fig. 2, slide onto the sphaleron-like configuration  $S'$ , which in turn eventually relaxes to the sphaleron itself. To avoid this, we add an additional term to the action that tends to pin the turning points, thereby halting the collapse into the sphaleron. We do this by minimizing an effective action of the form

$$S_{\text{eff}} = S + w_t (V_{N_t} - v_0)^2 , \quad (2.50)$$

where  $V_{N_t}$  is the potential energy on the final time slice,  $w_t$  is a weighting factor, and  $v_0$  is called the turning-point energy parameter. While the second term in (2.50) renders collapse to the sphaleron energetically unfavorable, in general the minima of  $S_{\text{eff}}$  are not the solutions we seek. However, if we choose the parameter  $v_0$  such that  $V_{N_t} = v_0$ , the minima of  $S_{\text{eff}}$  and  $S$  coincide. Thus, by adjusting  $v_0$  accordingly, we can find periodic instantons that do not collapse to the sphaleron.

The effective action (2.50) still typically fails to yield nontrivial periodic instantons. While the second term in (2.50) pushes the gradient search away from the static sphaleron, there is still another unstable direction. Rather than converging to

periodic instanton solutions, most initial guesses shrink to zero size. This is related to the fact that the standard model, with a nonzero vacuum expectation value, breaks conformal invariance and strictly speaking does not support instanton solutions (i.e., they shrink to zero size). We can remedy the situation by adding another term to the action that pins the zero of  $\chi(r, 0)$ , thereby halting the collapse of the configuration. We now consider the effective action

$$S_{\text{eff}} = S + w_t (V_{N_t} - v_0)^2 + w_{\text{zero}} [(1 - \alpha)\chi_{i,0} + \alpha\chi_{i+1,0}]^2, \quad (2.51)$$

where  $w_{\text{zero}}$  is another weighting factor. Just as before, we seek to minimize  $S_{\text{eff}}$ , but in addition to adjusting  $v_0$  so the second term of (2.51) vanishes, we also vary  $\alpha$  and  $i$  to give a vanishing third term (and hence the zero of  $\chi(r, 0)$  occurs at  $r_0 = (i + \alpha)\Delta r$ ).

A conjugate gradient minimization of the effective action (2.51), coupled with the two parameter search over  $v_0$  and  $\alpha$ , is a very effective method for obtaining periodic instantons. In this paper we only have space to present a typical solution, shown in Fig. 3, and a comprehensive treatment of periodic instantons in the  $\epsilon$ - $\nu$  plane must wait for a future publication.

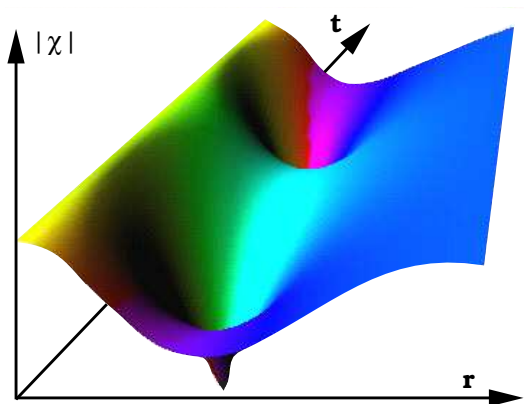


FIG. 3. Periodic Instanton: a full period of the  $\chi$ -field. The modulus of the field is represented by the height of the surface, while shades of gray code the phase.

### III. THE CLASSICALLY ALLOWED DOMAIN

We now examine the complimentary classically allowed regime above the sphaleron barrier, in which the solutions are purely real and propagate in Minkowski space-time. Finding these solutions is less computationally demanding than solving the tunneling problem of the previous section, while still yielding considerable information about baryon number violation. Spatial limitations prevent us from giving a full blown treatment of our numerical investigation, and the reader is referred to Ref. [3] for complete details. But the basic idea is that if a topology changing classical solution with small incident particle number could be found, this would be a strong indication that baryon number violation would be observable in high energy two-particle collisions. Conversely, if there are no small-multiplicity topology changing solutions, then it is unlikely that the rates become exponentially unsuppressed.

This can be made more precise in the following manner. Because of energy dissipation, the system will asymptotically approach vacuum values and will consequently linearize in the past and future. Field evolution then becomes a superposition of normal mode oscillators with amplitudes  $a_n$ , which allows us to define the asymptotic particle number  $\nu = \sum |a_n|^2$ . Furthermore, since the fields approach vacuum values in the infinite past and future, the winding numbers of the asymptotic field configurations are also well defined, and fermion number violation is given by the change in topology of these vacua [14]. Because of the sphaleron barrier, classical solutions that change topology must have energy  $\epsilon$  greater than that of the sphaleron. The problem we would like to solve, then, is whether the incident particle number  $\nu$  of these solutions can be made arbitrarily small. That is to say, we wish to map the region of topology changing classical solutions in the  $\epsilon$ - $\nu$  plane.

We could easily parameterize incoming configurations in terms of small perturbations about a given vacuum, but it would be extremely difficult to choose the

parameters to ensure a subsequent change in winding number. This is because topology changing classical solutions must pass over the sphaleron barrier at some point in their evolution, which is extremely difficult to arrange by an appropriate choice of initial conditions. So computationally, we pursue a different strategy. We will evolve a configuration near the top of the sphaleron barrier until it linearizes and the particle number can be extracted. The time reversed solution, then, has a known incident particle number and will typically pass over the sphaleron barrier thereby changing topology. Of course we have no obvious control over the asymptotic particle number of the initial sphaleron-like configuration; however, by using suitable stochastic sampling techniques, we can systematically lower the particle number while ensuring a change of topology. This will allow us to explore the  $\epsilon$ - $\nu$  plane and map the region of topology change, the lower boundary of which should tell us a great deal about baryon number violation in high energy collisions.

### A. Topological Transitions

Let us now put some flesh on the bones of the above discussion. As in the previous section, we still consider the standard model with zero Weinberg-angle, defined by action (2.38). As before, the coupling constant has been set to unity, but when needed it will be restored to its physical value of  $g = 0.652$ . We also take  $\lambda = 0.1$ , which corresponds to a Higgs mass of about  $M_H = 72 \text{ GeV}$ . Again we restrict ourselves to the spherical *Ansatz* (2.41), and examine the effective 1+1 dimensional  $U(1)$  theory (2.42).

Before investigating classical solutions of this effective theory, it is useful to first explore its topological structure, which is very similar to that of the full 4-dimensional theory. Vacuum states of the effective 2-dimensional theory are characterized by

$|\chi| = |\phi| = 1$  and  $i\chi^* \phi = -1$  (as well as  $D_\mu \chi = D_\mu \phi = 0$ ). The vacua then take the form

$$\begin{aligned}
a_{\mu \text{ vac}} &= \partial_\mu \Omega \\
\chi_{\text{vac}} &= -i e^{i\Omega} \\
\phi_{\text{vac}} &= \pm e^{i\Omega/2} ,
\end{aligned} \tag{3.1}$$

where the gauge function  $\Omega = \Omega(r, t)$  is required to vanish at  $r = 0$  to ensure regularity of the 4-dimensional fields. Furthermore, like the full 4-dimensional theory, these vacua still possess nontrivial topological structure. Compactification of 3-space requires that  $\Omega(r, t) \rightarrow 2\pi n$  as  $r \rightarrow \infty$ , in which case the winding number of such vacua in the  $a_0 = 0$  gauge is simply the integer  $n$ . Note that as  $r$  varies from zero to infinity,  $\chi$  winds  $n$  times around the unit circle while  $\phi$  only winds by half that amount.

Since the winding number is a topological invariant, a continuous path connecting two inequivalent vacua must at some point leave the manifold of vacuum configurations. Along this path there will be a configuration of maximal energy, and of all such maximal energy configurations there exists a unique one of minimal energy [7]. This configuration is called the sphaleron and may conveniently be parameterized by

$$\begin{aligned}
a_{\text{sph}}^\mu(r) &= 0 \\
\chi_{\text{sph}}(r) &= i[2f(r) - 1] \\
\phi_{\text{sph}}(r) &= ih(r) ,
\end{aligned} \tag{3.2}$$

where the profile functions  $f$  and  $h$  vanish at  $r = 0$ , and tend to unity as  $r \rightarrow \infty$  and are otherwise determined by minimizing the energy functional. The sphaleron energy is approximately  $M_w/g^2 \sim 10$  TeV, or  $\epsilon = 4\pi(2.54)$  for  $\lambda = 0.1$  in the units we are using (and it depends very weakly on the Higgs mass).

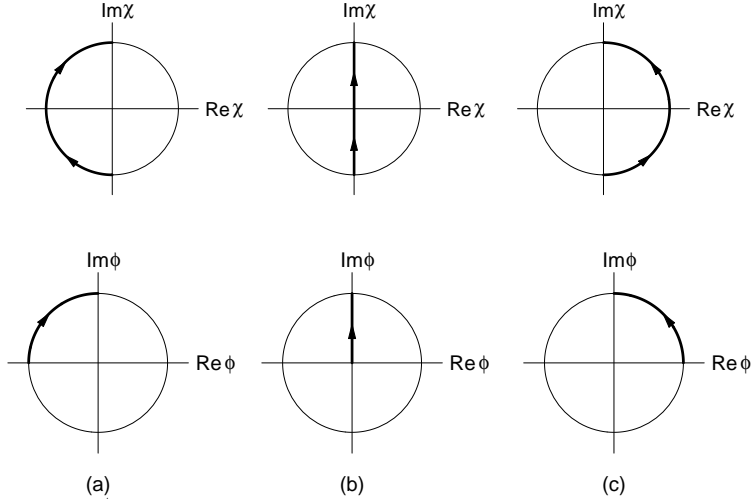


FIG. 4. The  $\chi$  and  $\phi$  fields for a vacuum-to-vacuum topology changing transition in a gauge inconsistent with compactified 3-space. The scalar fields are traced in the complex plane as the spatial coordinate spans the entire axis. Figs. (a) and (c) represent two inequivalent topological vacua while (b) is the sphaleron barrier separating them.

While the form of the sphaleron given by (3.2), in which  $a_\mu$  vanishes and  $\chi$  and  $\phi$  are pure imaginary, is convenient for numerical work, it does have a slight peculiarity. Recall that compactification of 3-space requires the gauge function  $U$  to approach an even multiple of  $2\pi$  as  $r \rightarrow \infty$ . It is possible to relax this restriction, and it will often be convenient to choose a gauge with  $U \rightarrow (2n+1)\pi$  as  $r \rightarrow \infty$ , in which case  $\chi_{\text{vac}} \rightarrow i$  and  $\phi_{\text{vac}} \rightarrow \pm i$ . This is precisely the large- $r$  boundary condition of the sphaleron, which illustrates that (3.2) is inconsistent with spatial compactification. There is of course nothing wrong with this, and a topological transition of unit winding number change in this gauge is illustrated in Fig. 4. Rather than  $\chi$  winding once around the unit circle, it instead winds over the left hemisphere before the transition and over the right after the transition. The total phase change is still  $2\pi$ , as it must be since this is a gauge invariant quantity.

Throughout most of this paper we shall use a gauge consistent with (3.2) in which space cannot be compactified. From a computational perspective, this will allow perturbations about the sphaleron to be more easily parameterized. There will,

however, be times when it is more convenient to impose spatial compactification, but we will always alert the reader to such a change of gauge.

## B. Classical Evolution

So far we have primarily been considering topology changing sequences of configurations, not necessarily solutions of the equations of motion. We now turn to the classical evolution of the system. We will consider solutions that linearize in the distant past and future, and hence those that asymptote to specific topological vacua. This allows us to define the incident particle number, and it makes clear what is meant by the topology change of a classical solution (namely, the change in winding number of the asymptotic vacua).

The field equations are coupled nonlinear particle differential equations and must be solved computationally on the lattice. But before we present our numerical procedure, we first formulate the problem in the continuum. The equations of motion resulting from the action (2.42) are

$$\partial^\mu (r^2 f_{\mu\nu}) = i [D_\nu \chi^* \chi - \chi^* D_\nu \chi] + \frac{i}{2} r^2 [D_\nu \phi^* \phi - \phi^* D_\nu \phi] \quad (3.3a)$$

$$\left[ D^2 + \frac{1}{r^2} (|\chi|^2 - 1) + \frac{1}{2} |\phi|^2 \right] \chi = -\frac{i}{2} \phi^2 \quad (3.3b)$$

$$\left[ D^\mu r^2 D_\mu + \frac{1}{2} (|\chi|^2 + 1) + 2\lambda r^2 (|\phi|^2 - 1) \right] \phi = i \chi \phi^* . \quad (3.3c)$$

The  $\nu = 0$  equation in (3.3a) is not dynamical but is simply the Gauss's law constraint.

To solve these equations, we must supplement them with boundary conditions. The conditions at  $r = 0$  can be derived by requiring the 4-dimensional fields to be regular at the origin. The behavior as  $r \rightarrow 0$  must be

$$a_0 = a_{0,1}r + a_{0,3}r^3 + \dots \quad (3.4a)$$

$$a_1 = a_{1,0} + a_{1,2}r^2 + \dots \quad (3.4b)$$

$$\alpha = \alpha_1r + \alpha_3r^3 + \dots \quad (3.4c)$$

$$\beta = -1 + \beta_2r^2 + \dots \quad (3.4d)$$

$$\mu = \mu_0 + \mu_2r^2 + \dots \quad (3.4e)$$

$$\nu = \nu_1r + \nu_3r^3 + \dots, \quad (3.4f)$$

where the coefficients of the  $r$ -expansion are undetermined functions of time. The  $r$ -behavior of the various terms are determined by the requirement that it has the appropriate power of  $r = (x^2 + y^2 + z^2)^{1/2}$  to render the 4-dimensional fields analytic in terms of  $x$ ,  $y$  and  $z$ . For example,  $a_0$  must be odd in  $r$  since  $A_0$  is proportional to  $a_0\boldsymbol{\sigma} \cdot \hat{\mathbf{x}} = (a_0/r)\boldsymbol{\sigma} \cdot \mathbf{x}$ . In terms of  $\chi$  and  $\phi$  the boundary conditions at  $r = 0$  become

$$a_0(0, t) = 0 \quad (3.5a)$$

$$\chi(0, t) = -i \quad (3.5b)$$

$$\text{Re } \partial_r \phi(0, t) = 0 \quad (3.5c)$$

$$\text{Im } \phi(0, t) = 0. \quad (3.5d)$$

There is another  $r = 0$  boundary condition which arises from the requirement that  $a_1 - \alpha/r$  be regular as  $r \rightarrow 0$ . In the notation of (3.4), this condition can be written as  $a_{1,0} = \alpha_1$ , and once imposed on initial configurations it remains satisfied at subsequent times because of Gauss's law.

We turn now to the large- $r$  boundary conditions. Finite energy configurations must approach pure vacuum at spatial infinity, and we may choose a gauge in which

$$a_\mu(r, t) \rightarrow 0 \quad (3.6a)$$

$$\chi(r, t) \rightarrow i \quad (3.6b)$$

$$\phi(r, t) \rightarrow i \quad (3.6c)$$

as  $r \rightarrow \infty$ . This choice of gauge does not admit spatial compactification, but nonetheless it is numerically convenient since it is consistent with the simple parameterization of the sphaleron (3.2). At times we will choose a gauge consistent with spatial compactification in which  $\chi(r, t) \rightarrow -i$  and  $\phi(r, t) \rightarrow 1$  as  $r \rightarrow \infty$ , but unless otherwise specified we will take the large- $r$  boundary conditions to be (3.6).

The field equations (3.3), together with boundary conditions (3.5) and (3.6), may now be used to evolve initial profiles and to investigate their subsequent topology change. The evolution is performed by discretizing the system using the methods of lattice gauge theory, in which we subdivide the  $r$ -axis into  $N$  equal intervals of length  $\Delta r$  with finite extent  $L = N\Delta r$  (in our numerical simulations we take  $N = 2239$  and  $\Delta r = 0.04$ ). The field theoretic system then becomes finite and may be solved using standard numerical techniques.

The fields  $\chi(r, t)$  and  $\phi(r, t)$  become discrete variables  $\chi_i(t)$  and  $\phi_i(t)$  associated with the lattice sites  $r_i = i\Delta r$  where  $i = 0 \cdots N$ . The continuum boundary conditions render the variables at the spatial end-points nondynamical, taking the values  $\chi_0 = -i$ ,  $\chi_N = i$  and  $\phi_N = i$  (the value of  $\phi_0$  will be discussed momentarily). The time component of the gauge field  $a_0(r, t)$  is also associated with the lattice sites and is represented by the variables  $a_{0,i}(t)$  with  $i = 0 \cdots N$ . We will usually work in the temporal gauge in which  $a_{0,i} = 0$ , and we will not concern ourselves with this degree of freedom.

The spatial components of the gauge field  $a_1(r, t)$  become discrete variables associated with the oriented links of the lattice, and we represent them by  $a_{1,i}(t) \equiv a_i(t)$  located at positions  $r_{i+1/2} = (i + 1/2)\Delta r$  with  $i = 0 \cdots N - 1$ . The covariant spatial derivatives become covariant finite difference operators that are also associated with the links, e.g.

$$D_r \phi \rightarrow \frac{\exp[-ia_i \Delta r/2] \phi_{i+1} - \phi_i}{\Delta r} \quad i = 0 \cdots N - 1, \quad (3.7)$$

where  $a_i$  is short-hand notation for  $a_{1,i}$ .

It is now straightforward to discretize the action (2.42) in a manner that still possesses an exact local gauge invariance. But first, we need to state the restriction on  $\phi_0(t)$  corresponding to the boundary conditions (3.5c) and (3.5d). Since  $a_1$  is real, we can write these boundary conditions in a covariant fashion by requiring the real part of  $D_r\phi$  and the imaginary part of  $\phi$  to vanish at  $r = 0$ . Using the discretized operator (3.7), we can then solve this boundary condition for  $\phi_0$  to obtain

$$\phi_0 = \text{Re} [\exp(-i a_0 \Delta r/2)\phi_1] , \quad (3.8)$$

where  $a_0$  is the value of  $a_{1,i}$  at  $i = 0$  and should not be confused with the time-like vector field. This now allows us to eliminate  $\phi_0$  from the list of dynamical variables.

Finally, the discretized Lagrangian becomes

$$\begin{aligned} L = & 4\pi \sum_{i=0}^{N-1} \left\{ \frac{r_{i+1/2}^2}{2} \left( \partial_0 a_i - \frac{a_{0,i+1} - a_{0,i}}{\Delta r} \right)^2 - \frac{|\exp(-i a_i \Delta r)\chi_{i+1} - \chi_i|^2}{\Delta r^2} \right\} \Delta r \\ & + 4\pi \sum_{i=1}^{N-1} \left\{ |(\partial_0 - i a_{0,i})\chi_i|^2 + r_i^2 |(\partial_0 - \frac{i a_{0,i}}{2})\phi_i|^2 - r_{i+1/2}^2 \frac{|\exp(-i a_i \Delta r/2)\phi_{i+1} - \phi_i|^2}{\Delta r^2} \right. \\ & \left. - \frac{1}{2} (|\chi_i|^2 + 1)|\phi_i|^2 - \text{Re}(i\chi_i^* \phi_i^2) - \frac{1}{2r_i^2} (|\chi_i|^2 - 1)^2 - \lambda r_i^2 (|\phi_i|^2 - 1)^2 \right\} \Delta r \\ & - 4\pi r_{1/2}^2 \frac{[\text{Im}(\exp(-i a_0 \Delta r/2)\phi_1)]^2}{\Delta r} , \end{aligned} \quad (3.9)$$

and the system may now be evolved using standard numerical techniques of ordinary differential equations. The Lagrangian (3.9) is actually of a Hamiltonian type with no dissipative terms, so it is convenient to use the leapfrog algorithm to perform the numerical integration.

We do not have space to outline this well known computational procedure, so instead we simply state some of its more attractive features. First, the algorithm is second order accurate (i.e. the error from time discretization is of order  $(\Delta t)^3$  in the individual steps and of order  $(\Delta t)^2$  in an evolution of fixed length  $L = N\Delta r$ ). Second,

energy is exactly conserved in the linear regime, a desirable feature when pulling out the particle number. And finally, the algorithm possesses an exact discretized-time invariance, which is important since we are interested in obtaining the time reversed solutions starting from perturbations about the sphaleron. Of course these last two properties hold exactly only up to round-off errors, which can be made quite small by using double precision arithmetic.

### C. The Initial Configuration: Perturbation About the Sphaleron

We are now ready to continue our investigation into the connection between the incident particle number of a classical solution and subsequent topology change. We could proceed by parameterizing linear incoming configurations of known particle number, but it would be extremely difficult to arrange the classical trajectory to traverse the sphaleron barrier. If we failed to see topology change for a given initial configuration, we could never be sure whether it was simply forbidden in principle by the choice of incident particle number, or simply because the initial trajectory was pointed towards the wrong direction in field space.

To alleviate this difficulty, we have chosen to evolve initial configurations at or near the moment of topology change, and when the linear regime is reached the particle number will be extracted in the manner explained shortly. The physical process of interest is then the time reversed solution that starts in the linear regime with known particle number and subsequently proceeds over the sphaleron barrier. Of course we must explicitly check whether topology change in fact occurs, but we have found that it usually does. Fig. 5 illustrates the numerical evolution of the  $\chi$  field for a typical topology changing solution obtained in this manner. The modulus of  $\chi$  is represented by the height of the surface, while the phase is color coded (but unfortunately we can only reproduce the figure in gray scale). We have reverted to a gauge where  $\chi_N = -i$

and  $\phi_N = 1$ , consistent with spatial compactification, and in which the incoming state has no winding and the outgoing state has unit winding number. The topology change is represented by the persistent strip of  $2\pi$  phase change near the origin after the transition.

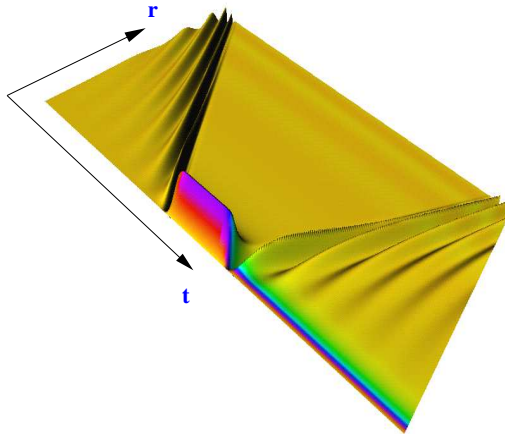


FIG. 5. Topology changing transition: behavior of the  $\chi$  field obtained the time reversal procedure described in the text. The various shades of gray code the phase of the complex field. The field starts as an excitation about the trivial vacuum, passes over the sphaleron and then emerges as an excitation about the vacuum of unit winding. Note the persistent strip of  $2\pi$  phase change near  $r = 0$  after the wave bounces off the origin.

We turn now to parameterizing initial configurations. For classical solutions that dissipate in the past and future, topology change (and hence baryon number violation) is characterized by zeros of the Higgs field [14]. For such topology changing solutions in the spherical *Ansatz*, the  $\chi$  field, which parameterizes the transverse gauge degrees of freedom, must also vanish at some point in its evolution. However, unless the transition proceeds directly through the sphaleron, the zeros of  $\phi$  and  $\chi$  need not occur simultaneously, and for convenience we shall choose to parameterize the initial configuration at the time when  $\chi$  vanishes for some nonzero  $r$ . Furthermore, we can exhaust the remaining gauge freedom by taking the initial  $\chi$  to be pure imaginary. We thus parameterize the initial conditions as an expansion in terms of some appropriate

complete set with coefficients  $c_n$ , consistent only with the boundary conditions and the requirement that  $\chi$  be pure imaginary with a zero at some  $r > 0$ .

We choose to parameterize initial conditions in terms of perturbations about the sphaleron given by linear combinations of spherical Bessel functions consistent with the small- $r$  behavior (3.4). We only need the first three functions

$$j_0(x) = \frac{\sin x}{x} \quad (3.10a)$$

$$j_1(x) = \frac{\sin x}{x^2} - \frac{\cos x}{x} \quad (3.10b)$$

$$j_2(x) = \left( \frac{3}{x^3} - \frac{1}{x} \right) \sin x - \frac{3}{x^2} \cos x , \quad (3.10c)$$

since  $j_0(x) \sim 1$ ,  $j_1(x) \sim x$  and  $j_2(x) \sim x^2$  at small  $x$ . We also require the perturbations to vanish at  $r = L$  consistent with the large- $r$  boundary conditions (3.6). We then parameterize perturbations about the sphaleron in terms of  $j_{nm}(r) = j_n(\alpha_{nm}r)$  with  $n = 0, 1, 2$ , where  $\alpha_{nm}$  with  $m = 1, 2, \dots$  are the zeros of  $j_n(x)$ . We are thus led to parameterize the initial conditions as

$$\chi(r, 0) = \chi_{\text{sph}}(r) + i \sum_{m=1}^{N_{\text{sph}}} c_{1m} j_{2m}(r) \quad (3.11a)$$

$$\phi(r, 0) = \phi_{\text{sph}}(r) + \sum_{m=1}^{N_{\text{sph}}} c_{2m} j_{0m}(r) + i \sum_{m=1}^{N_{\text{sph}}} c_{3m} j_{1m}(r) \quad (3.11b)$$

$$\dot{\chi}(r, 0) = \sum_{m=1}^{N_{\text{sph}}} c_{4m} j_{1m}(r) + i \sum_{m=1}^{N_{\text{sph}}} c_{5m} j_{2m}(r) \quad (3.11c)$$

$$\dot{\phi}(r, 0) = \sum_{m=1}^{N_{\text{sph}}} c_{6m} j_{0m}(r) + i \sum_{m=1}^{N_{\text{sph}}} c_{7m} j_{1m}(r) \quad (3.11d)$$

$$a_1(r, 0) = \sum_{m=1}^{N_{\text{sph}}} c_{8m} j_{2m}(r) , \quad (3.11e)$$

where  $\chi_{\text{sph}}$  and  $\phi_{\text{sph}}$  are the sphaleron profiles, and where the sum is cut off at  $N_{\text{sph}} \leq N$ . To avoid exciting short wave length modes corresponding to lattice artifacts, we shall take  $N_{\text{sph}} \sim N/50$  (in our numerical work,  $N_{\text{sph}} = 50$  for  $N = 2239$ ).

We have used continuum notation, but (3.11) is to be thought of as defining  $\chi$  and  $\phi$  on the lattice sites  $r_i$  and  $a_1$  on the links  $r_{i+1/2}$ . The time derivative of  $a_1$  is to be determined by Gauss's law.

#### D. Normal Modes and Particle Number

We are now in a position to discuss the manner in which the asymptotic particle number is to be extracted. Recall that once the system has reached the linear regime it can be represented as a superposition of normal modes, and the particle number can be defined as the sum of the squares of the normal mode amplitudes. Since we have put the system on a lattice, we should properly calculate these amplitudes using the exact normal modes of the discrete system. However, since our lattice is very dense ( $N = 2239$  with  $\Delta r = 0.04$ ), it suffices to project onto the normal modes of the corresponding continuum system of finite extent  $L = N\Delta r$ , the advantage being that we can solve for the continuum normal modes analytically. We have checked that this procedure agrees extremely well with projecting onto normal modes of the discrete system (obtained numerically), so for clarity we present only the continuum modes.

It is convenient to work in terms of the gauge invariant variables of Ref. [16]. We write the fields  $\chi$  and  $\phi$  in polar form,

$$\chi = -i [1 + y] e^{i\theta} \tag{3.12}$$

$$\phi = \left[ 1 + \frac{h}{r} \right] e^{i\eta} , \tag{3.13}$$

where the variables  $y$  and  $h$  are gauge invariant. We can also define the gauge invariant angle

$$\xi = \theta - 2\eta , \tag{3.14}$$

and in 1+1 dimensions we can define a gauge invariant quantity  $\psi$  through

$$r^2 f_{\mu\nu} = -2\epsilon_{\mu\nu}\psi , \quad (3.15)$$

where  $\epsilon_{01} = +1$  and  $\mu, \nu$  run over 0 and 1. Rather than working with the six gauge-variant degrees of freedom  $\chi, \phi$  and  $a_\mu$  we use the four gauge invariant variables  $h, y, \psi$  and  $\xi$ .

We wish to find the equations of motion for small linearized fluctuations about the vacuum. In gauge invariant coordinates the vacuum takes the form  $h_{\text{vac}} = y_{\text{vac}} = \psi_{\text{vac}} = \xi_{\text{vac}} = 0$ , and we thus need only work to linear order in the variables. From Ref. [16] the normal mode equations are

$$\left( \partial_\mu \partial^\mu + 4\lambda \right) h = 0 \quad (3.16a)$$

$$\left( \partial_\mu \partial^\mu + \frac{1}{2} + \frac{2}{r^2} \right) y = 0 \quad (3.16b)$$

$$\partial^\mu \left\{ \frac{\partial_\mu \psi - \epsilon_{\mu\nu} \partial^\nu \xi}{1 + \frac{1}{4}r^2} \right\} + \frac{2}{r^2} \psi = 0 \quad (3.16c)$$

$$\partial^\mu \left\{ \frac{\frac{1}{4}r^2 \partial_\mu \xi + \epsilon_{\mu\nu} \partial^\nu \psi}{1 + \frac{1}{4}r^2} \right\} + \frac{1}{2} \xi = 0 . \quad (3.16d)$$

Equation (3.16a) corresponds to a pure Higgs excitation characterized by mass  $M_H = 2\sqrt{\lambda}$ , while (3.16b)-(3.16d) correspond to three gauge modes of mass  $M_W = 1/\sqrt{2}$ . \*

Note that there are four types of normal modes. The first two are easily obtained by solving the independent equations (3.16a) and (3.16b), while the last two can be found by solving the coupled equations (3.16c) and (3.16d) involving  $\psi$  and  $\xi$ . A solution in the linear regime can then be expanded as a combination of these four modes and the amplitudes  $a_{kn}$  extracted, where  $k = 1, 2, 3, 4$  specifies the mode type. The Higgs and gauge particle numbers are defined by

---

\*Upon restoring the factors of  $g$  and the Higgs vacuum expectation value  $v$ , these masses take the standard form  $M_H = \sqrt{2\lambda}v$  and  $M_W = (1/2)gv$ .

$$\nu_{\text{higgs}} = \sum_{n=1}^{N_{\text{mode}}} |a_{1n}|^2 \quad (3.17)$$

$$\nu_{\text{gauge}} = \sum_{n=1}^{N_{\text{mode}}} \left\{ |a_{2n}|^2 + |a_{3n}|^2 + |a_{4n}|^2 \right\} , \quad (3.18)$$

with total particle number given by

$$\nu = \nu_{\text{higgs}} + \nu_{\text{gauge}} . \quad (3.19)$$

To avoid counting lattice artifacts we take the ultraviolet cutoff on the mode sums to be  $N_{\text{mode}} \sim N/5$  to  $N/10$ .

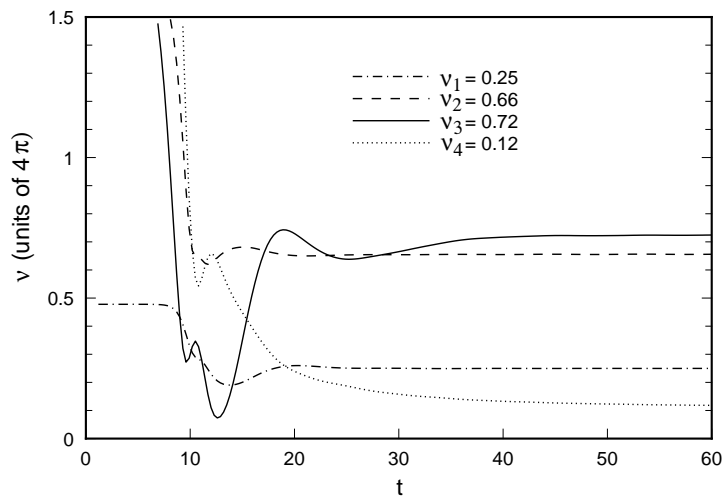


FIG. 6. Decay of a small perturbation about the sphaleron: behavior of the particle number in the four modes as function of time for lattice parameters  $N = 2239$ ,  $\Delta r = 0.04$  and  $N_{\text{mode}} = 200$  with  $\lambda = 0.1$ . The physical particle numbers are obtained by multiplying the asymptotic values in the graph by  $4\pi/g^2 \sim 30$ , which gives  $N_{\text{higgs}} \sim 8$  and  $N_{\text{gauge}} \sim 45$ , for a total physical particle number of  $N_{\text{phys}} \sim 53$ .

Space does not permit a detailed exposition of this procedure, and one should consult Ref. [3] for full details. Here we must be content with Fig. 6, which displays the behavior of the particle number in the four normal modes as a function of time. As an initial state we chose a typical perturbation about the sphaleron as described in the previous section, and we see that its evolution quickly linearizes and settles down into a definite asymptotic particle number.

## E. Stochastic Sampling of Initial Configurations

Recall that our computational strategy consists in evolving a configuration near the top of the sphaleron barrier until it linearizes, at which point the particle number is extracted and the time reversed solution is then used to generate the topology changing process of interest. We can regard the energy  $\epsilon$  and the asymptotic particle number  $\nu$  as functions of the parameters  $c_n$  that specify the initial configuration, and by varying these coefficients we would like to explore the  $\epsilon$ - $\nu$  plane and attempt to map the region of topology change. In particular, for a given energy  $\epsilon$ , we would like to find the minimum allowed particle number  $\nu_{\min}(\epsilon)$  consistent with a change of topology. If this number can be made arbitrarily small, this would be a strong indication that baryon number violation would be observable in a two-particle collision.

By randomly exploring the initial configuration space, parameterized by the coefficients  $c_n$ , we would stand little chance of making headway. Instead, we shall employ stochastic sampling techniques, which are ideal for tackling this type of multi-dimensional minimization. Our procedure will be to generate initial configurations weighted by  $W = \exp(-F)$  with  $F = \beta\epsilon + \mu\nu$ , and by adjusting the parameters  $\beta$  and  $\mu$  we can explore selected regions in the  $\epsilon$ - $\nu$  plane. In particular, by increasing  $\mu$  we can drive the system to lower and lower values of  $\nu$  for a given  $\epsilon$ . In our numerical work we typically take  $\beta$  between 50 and 1000 while  $\nu$  ranges between 1000 to 20000.

To generate the desired distributions we have used a Metropolis Monte-Carlo algorithm. Starting from a definite configuration parameterized by  $c_n$ , we perform an upgrade to  $c_n \rightarrow c'_n = c_n + \Delta c_n$  where  $\Delta c_n$  is Gaussian distributed with a mean of about 0.0008. We evolve the updated configuration until it linearizes and then calculate  $\Delta F = \beta \Delta\epsilon + \mu \Delta\nu$ . If the topology of the physically relevant time reversed solution does not change, then we discard the updated configuration. Otherwise we accept it with conditional probability  $p = \text{Min}[1, \exp(-\Delta F)]$ , which is equivalent to

always accepting configurations that decrease  $F$  while accepting those that increase  $F$  with conditional probability  $\exp(-\Delta F)$ .

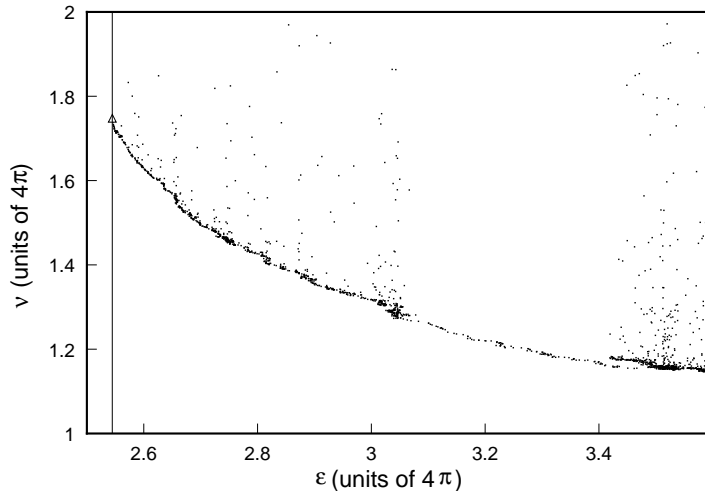


FIG. 7. Monte Carlo results with lattice parameters of  $N = 2239$ ,  $\Delta r = 0.04$  (giving  $L=89.56$ ),  $N_{\text{mode}} = 200$  and  $N_{\text{sph}} = 50$ , and with a Higgs self-coupling of  $\lambda = 0.1$ . The solid line marks the sphaleron energy  $\epsilon_{\text{sph}} = 4\pi(2.5426)$ , below which no topology changing process can lie. The triangle represents the configuration from which we seeded our Monte Carlo search. To obtain quantities in physical units, multiply the numbers along the axes by  $4\pi/g^2 \sim 30$ . The energy axis extends from about 10 TeV to 15 TeV, while the particle number axis ranges from about 30 particles to 60.

We are now in a position to present our numerical results. Fig. 7 represents 300 CPU hours and involves 30000 solutions (of which only 3000 are shown) obtained on the CM-5, a 64 node parallel supercomputer. We have chosen the lattice parameters  $N = 2239$ ,  $\Delta r = 0.04$ , with ultraviolet cutoffs determined by  $N_{\text{sph}} = 50$  and  $N_{\text{mode}} = 200$ . The Higgs self-coupling was taken to be  $\lambda = 0.1$ , which corresponds to a Higgs mass of  $M_H = 72$  GeV.

We have managed to produce a marked decrease of about 40% in the minimum particle number  $\nu_{\text{min}}(\epsilon)$ , which is approximated by the lower boundary in the Fig. 7. Nowhere, however, in the explored energy range does  $\nu$  drop below  $4\pi$ , or in physical units the incident particle number  $N \geq 30$  for energy  $E \leq 15$  TeV (the outgoing particle number tends to be about 50 to 100). This is a far cry from two incoming par-

ticles which would be necessary to argue that baryon number becomes unsuppressed in high energy collisions.

The complex nature of the solution space can be illustrated by the break in population density between  $\epsilon/4\pi \sim 3$  and  $\epsilon/4\pi \sim 3.4$ . In our first extended search we did not check whether topology change actually occurred, trusting that the time reversed solutions would continue over the sphaleron barrier. However, we later found an entire region between  $\epsilon/4\pi \sim 3$  and  $\epsilon/4\pi \sim 3.4$  in which the solutions never left the original topological sector. We excluded these points and restarted our search procedure near  $\epsilon/4\pi \sim 3$ . A small discontinuity in the lower boundary with slightly lower particle number was produced, but we have still managed to approximate  $\nu_{\min}(\epsilon)$  remarkably well.

We can extract more information from the system by investigating the asymptotic spectral distribution  $|a_{kn}|^2$  as a function of mode number  $n$ . Before we started the search, our seed configuration (represented by the triangle in Fig. 7) linearized into a distribution that was heavily peaked about a small mode number  $n_{\text{pk}} \sim 50$  (with  $\Delta n \sim 50$ ), corresponding to a frequency of  $\omega_{\text{pk}} \sim \pi n_{\text{pk}}/L \sim 0.1$ . After the search the solutions underwent a dramatic mode redistribution. The amplitudes  $|a_{kn}|^2$  of the linear regime peaked at higher mode number,  $n_{\text{pk}} \sim 75 - 100$ , with a much broader distribution ( $\Delta n \sim 200$ ). Clearly our search procedure is very efficient in redistributing the mode population density.

While  $\nu$  remains large throughout the energy range we have explored, it is interesting to note that  $\nu_{\min}(\epsilon)$  maintains a slow but steady decrease with no sign of leveling off. To obtain an indication of the possible behavior of  $\nu_{\min}(\epsilon)$  at higher energies, we performed fits to our data using functional forms which incorporate expected analytical properties of the boundary of the domain of topology changing solutions. The fits gave a particle number  $N = 2$  at energies in the range of 100 TeV to 450 TeV. Of course we must explore higher energies before drawing definite conclusions, but this is at least suggestive that particle number might at some point become small.

## IV. CONCLUSIONS

We have reviewed in some detail the semiclassical method proposed by Rubakov, Son, and Tinyakov (RST) for bounding the exponential behavior of the two-particle baryon number violating cross section in the standard model. There are two distinct regimes, one in which the solutions that saturate the functional integral are real, corresponding to classically allowed processes above the sphaleron barrier, and another regime in which the saddle-point solutions are complex, representing Minkowski evolution followed by Euclidean tunneling under a barrier. In both cases, a topology changing solution of small incident particle number would be a signal that two-particle baryon number violating rates would be observable in high energy scattering experiments.

Finding the aforementioned saddle-point solutions is a formidable numerical task, but we have nonetheless made considerable progress, and in these lectures we have presented some of our initial computational results. In the Minkowski regime above the sphaleron barrier, we evolve nonlinear configurations at the moment of topology change until the system linearizes, at which point the asymptotic particle number can be extracted. The time reversed solutions, which have known incident particle numbers, will typically undergo topology change, and our computational strategy is to stochastically search the space of such topology changing solutions weighted for small incoming particle number. We have found that our numerical algorithm is extremely efficient in sifting configurations of smaller and smaller incident particle number. Starting with a generic perturbation of the sphaleron, which decayed into about 50 particles, we have managed to lower the particle number by 40%, to approximately 30 particles, while still maintaining topology change. Even though this number is rather large, we have only covered a narrow energy range, from 10 TeV to 15 TeV, but still

it is noteworthy that over this domain the data show a slow but steady decrease in incident particle number as the energy increases. In an effort to increase the rate at which we can collect numerical data, we have continued our search on a lattice with half the number of sites. This new lattice is sufficiently dense to ensure adequate linearization, but with much less CPU time, and we soon hope to have results well beyond the energy range we have explored to date.

Computational methods for finding the saddle-points in the classically forbidden regime are more involved than the above stochastic procedure. These solutions, which can become complex along the Euclidean-time axis, satisfy rather complicated boundary conditions, and we are still developing a procedure robust enough to find the general RST saddle-point. The periodic instanton of Ref. [9] is a special case of these tunneling saddle-points, and it has the advantage that it remains real along the entire Euclidean axis and satisfies rather simple turning-point boundary conditions. In these lectures we have been content with presenting a computational procedure to solve for the periodic instanton based on conjugate gradient minimization, and we have presented a typical numerical solution.

## Acknowledgments

C.R. was supported in part under DOE grant DE-FG02-91ER40676. R.S. was supported in part under DOE grant DE-FG03-96ER40956 and NSF grant ASC-940031. We wish to thank V. Rubakov for very interesting conversations which stimulated the investigation described here, and P. Arnold, A. Cohen, K. Rajagopal, D. Son, and P. Tinyakov for valuable discussions.

---

- [1] A. Ringwald, *Nucl. Phys.* **B330**, (1990) 1.
- [2] O. Espinosa, *Nucl. Phys.* **B343**, (1990) 310.
- [3] C. Rebbi and R. Singleton, Jr., *Phys. Rev.* **D54**, (1996) 1020, hep-ph/9601260.
- [4] V. Rubakov, D. Son and P. Tinyakov, *Phys. Lett.* **B287**, (1992) 342.
- [5] R. Jackiw and C. Rebbi, *Phys. Rev. Lett.* **37**, (1976) 172; C. Callan Jr., R. Dashen, and D. Gross, *Phys. Lett.* **63B**, (1976) 334.
- [6] G. 't Hooft, *Phys. Rev.* **D14**, (1976) 3432.
- [7] N. Manton, *Phys. Rev.* **D28**, (1983) 2019;  
F. Klinkhamer and N. Manton, *Phys. Rev.* **D30**, (1984) 2212.
- [8] V. Kuzmin, V. Rubakov, and M. Shaposhnikov, *Phys. Lett.* **B155**, (1985) 36.
- [9] S. Khlebnikov, V. Rubakov, and P. Tinyakov, *Nucl. Phys.* **B 367**, (1991) 334.
- [10] S. Khlebnikov, V. Rubakov, and P. Tinyakov, *Nucl. Phys.* **B 350**, (1991) 441.
- [11] P. Tinyakov, *Phys. Lett. B* **284**, (1992) 410.
- [12] V. Rubakov and P. Tinyakov, *Phys. Lett.* **B279**, (1992) 165.
- [13] H. Aoyama and H. Goldberg, *Phys. Lett. B* **188**, (1987) 506; H. Goldberg, *Phys. Lett. B* **257**, (1991) 346; S. Khlebnikov, A. Rubakov, and P. Tinyakov, *Nucl. Phys.* **B367**, (1991) 310.
- [14] E. Farhi, J. Goldstone, S. Gutmann, K. Rajagopal and R. Singleton Jr., *Phys. Rev.* **D51**, (1995) 4561, hep-ph/9410365.
- [15] B. Ratra and L. Yaffe, *Phys. Lett.* **B205**, (1988) 57.
- [16] E. Farhi, K. Rajagopal and R. Singleton Jr., *Phys. Rev.* **D52**, (1995) 2394, hep-ph/9503268.